Mechanism of SOA formation determines magnitude of radiative effects

Jialei Zhu[a], Joyce E. Penner[a,1], Guangxing Lin[b], Cheng Zhou[a], Li Xu[c], and Bingliang Zhuang[d]

[a]Department of Climate and Space Sciences and Engineering, University of Michigan, Ann Arbor, MI 48109; [b]Atmospheric Sciences and Global Change Division, Pacific Northwest National Laboratory, Richland, WA 99354; [c]Department of Earth System Science, University of California, Irvine, CA 92697; and [d]School of Atmospheric Sciences, Nanjing University, Nanjing, Jiangsu Province 210023, China

Edited by Piers M. Forster, University of Leeds, Leeds, United Kingdom, and accepted by Editorial Board Member A. R. Ravishankara October 24, 2017 (received for review July 11, 2017)

Secondary organic aerosol (SOA) nearly always exists as an internal mixture, and the distribution of this mixture depends on the formation mechanism of SOA. A model is developed to examine the influence of using an internal mixing state based on the mechanism of formation and to estimate the radiative forcing of SOA in the future. For the present day, 66% of SOA is internally mixed with sulfate, while 34% is internally mixed with primary soot. Compared with using an external mixture, the direct effect of SOA is decreased due to the decrease in total aerosol surface area and the increase of absorption efficiency. Aerosol number concentrations are sharply reduced, and this is responsible for a large decrease in the cloud albedo effect. Internal mixing decreases the radiative effect of SOA by a factor of >4 compared with treating SOA as an external mixture. The future SOA burden increases by 24% due to CO_2 increases and climate change, leading to a total (direct plus cloud albedo) radiative forcing of −0.05 W m^{-2}. When the combined effects of changes in climate, anthropogenic emissions, and land use are included, the SOA forcing is −0.07 W m^{-2}, even though the SOA burden only increases by 6.8%. This is caused by the substantial increase of SOA associated with sulfate in the Aitken mode. The Aitken mode increase contributes to the enhancement of first indirect radiative forcing, which dominates the total radiative forcing.

SOA | mixing state | radiative effects | future climate

Secondary organic aerosol (SOA) can be formed via gas-phase reactions and the subsequent condensation of semivolatile vapor, as well as by multiphase and heterogeneous processes (1). SOA accounts for as much as 50–85% of the total organic aerosol (OA) burden (2). As a result, SOA also contributes importantly to the Earth's radiation balance through its absorption and scattering of solar radiation and by altering cloud microphysical properties (3). However, significantly different treatments for formation of SOA among different models (4) are expected to lead to different estimates of its radiative effect.

Particle size, shape, and composition determine the optical properties of aerosols (5), their cloud condensation nuclei activity (6), and atmospheric lifetime (7), so it is important to model the distribution of chemical species within various aerosols or the mixing state to predict radiative forcing and burden. Recent observations using single-particle measurement techniques have found that particles can acquire coatings rapidly, sometimes within a few hours, and hence a sizable fraction of total ambient aerosols exist as internal mixtures (8–10). Direct measurements of the mixing state for SOA are very limited, but many studies have demonstrated that more than 75% of carbonaceous particles are internally mixed with secondary species like sulfate, ammonium, or nitrate in both polluted and remote areas, and at all altitudes (9–11). Despite the importance of the distribution and mixing state, some atmospheric models still represent the particle population as an external mixture (12–14), especially since the formation of SOA is associated with complex and not fully understood mechanisms (1, 15, 16). However, an external mixing assumption is unrealistic for many atmospheric situations (17, 18). Models without a full range of SOA formation mechanisms that also track the association of SOA with other aerosols during formation will therefore differ significantly in their predicted radiative effects.

Semivolatile gas-phase organic species are distributed to preexisting particles generally through either thermodynamic equilibrium (19–21) or kinetically controlled processes (22, 23) in models that treat SOA using internal mixtures. However, the use of only the thermodynamic approach is unable to account for the growth of small particles and the kinetic approach should only be used for organic oxidation products with low volatility or that form on aerosols through heterogeneous processes (24–26). Therefore, a comprehensive approach is needed to fully describe the distribution of different organic species within aerosols. This requires a representation of explicit organic chemical oxidation processes. Many models assume empirical or semiempirical fixed total SOA yields from monoterpene and isoprene oxidation rather than including a full chemical pathway for formation (4, 21, 23, 27), which affects the spatial distribution and size of SOA as well as the time scale for SOA formation.

A large range of up to 1 W m^{-2} in the radiative effects of SOA was estimated by different models, especially for the first aerosol indirect effect (AIE) (also termed the cloud albedo effect). The uncertainty in the magnitude and even the sign (cooling or warming) is partly associated with the different approaches used to estimate the mixing state of SOA (3, 14, 21). The aerosol direct radiative effect (DRE) of SOA is less sensitive to the method used to distribute organic species among aerosols than is the AIE since the DRE responds more to changes in SOA

Significance

Secondary organic aerosol (SOA) forms via a variety of processes and plays a key role in climate change and air quality. Recent measurements indicate that most SOA exists as an internal mixture with other aerosols. This study examines the radiative effect of using a mixing state for SOA that depends on the process of formation, based on an explicit mechanism for the chemical production of SOA. The radiative forcing of SOA in the future is estimated using this approach. A surprising result is that the contribution of SOA to radiative forcing increases substantially (becomes more negative) in the future even though the increase of its burden is slight.

Author contributions: J.Z. and J.E.P. designed research; J.Z., G.L., C.Z., and L.X. performed research; J.Z., J.E.P., and B.Z. analyzed data; and J.Z. and J.E.P. wrote the paper.

The authors declare no conflict of interest.

This article is a PNAS Direct Submission. P.M.F. is a guest editor invited by the Editorial Board.

[1]To whom correspondence should be addressed. Email: penner@umich.edu.

This article contains supporting information online at www.pnas.org/lookup/suppl/doi:10.1073/pnas.1712273114/-/DCSupplemental.

formation source strengths rather than its microphysical complexities (28). However, based on studies of soot mixed with other components (29, 30), one expects that the manner and degree of mixing of SOA will be important in its absorption and DRE.

The burden of anthropogenic aerosols is projected to decline strongly during the 21st century as governments enact and enforce stricter emission control policies (31). However, the burden of SOA is expected to increase due to nonlinear interactions in climate, anthropogenic emissions, and land use (32). Thus, SOA may play an important role in aerosol radiative forcing (RF) in the future. As we show here, the mixing and distribution state of SOA is an important factor needed to quantify its RF both currently and in the future.

This study uses the application of a comprehensive distribution approach for organic species from different formation mechanisms based on an explicit mechanism for gaseous- and aqueous-phase chemical production. We first examine the contrasting burdens as well as direct and first indirect radiative effects of SOA due to internal vs. external treatments for its mixing state. Then we quantify the RF of SOA in the future due to its change in mixing state and size distribution. Our results show that there is a significant influence on the estimated radiative effects of SOA due to different treatments for SOA mixing and show that its future RF depends strongly on its mixing state and size distribution.

Results and Discussion

Influence of Mixing on SOA Burden. Table 1 summarizes the distribution of SOA in each scheme. The external mixing (EM) scheme treats SOA as an externally mixed organic particle with sulfate coatings on the surface. In the internal mixing (IM) and IM_OC (organic carbon) schemes, SOA is internally mixed with sulfate, soot, dust, and sea salt based on its formation mechanism. The details of these schemes are described in *Methods* and *SI Appendix*, section S1. As a result of both the large concentration of sulfate aerosols compared with other types and SOA formation through kinetic uptake of glyoxal, methylglyoxal, and epoxides on sulfate aerosol surfaces, 66% of SOA is associated with the pure-sulfate aerosols in the IM scheme. Measurements also indicate that it is common to find organic aerosols that are internally mixed with sulfate (11, 17). On average 50.1% of the SOA is associated with sulfate in the accumulation mode due to its dominant mass concentration and total surface area. Only a small amount (2%) of SOA is associated with nucleation mode sulfate. The percentages of SOA mixed with sulfate vary spatially with relatively higher concentrations in most continental regions, although higher percentages of SOA mixed with sulfate in the nucleation and Aitken modes are found in remote areas (Fig. 1). SOA formed from isoprene epoxides (IEPOX) is high over land areas and accounts for 30.4% of total SOA on average, with a maximum of over 50% occurring in the tropics. This source makes a 46% contribution to the percentage of SOA mixed with sulfate. Most of the rest of the SOA (not associated with sulfate) condenses on and is internally mixed with soot, which accounts for 34% of the total SOA. The spatial distribution of the percentage of SOA mixed with soot is opposite that of SOA mixed with sulfate with maxima over the oceans in the Northern Hemisphere where there is little SOA formed from IEPOX as well as in China and India, which have the highest concentration of fossil-fuel-burning soot (fSoot) (Fig. 1). The percentage of average SOA condensed on fSoot is close to that of the average SOA condensed on biomass-burning soot (bSoot), but with a quite different spatial distribution. The percentage of SOA mixed with bSoot in the middle of Africa and South America is much higher than SOA mixed with fSoot, due to the large emission sources of bSoot over Africa and South America. The amount of SOA mixed with other aerosol types (i.e., sea salt and dust) is small (only about 0.2%).

The IM_OC scheme was designed as a sensitivity test to consider observations that showed that OC from anthropogenic sources can be nonliquid even at high relative humidity (RH) and exist in an EM state in the Amazon (33). Thus, these particles would not participate in thermodynamic processes that allow semivolatile gases to partition to the particle phase. SOA formed from traditional gas-particle partitioning and irreversible aerosol-phase reactions on primary organic aerosols is mixed with OC in the IM scheme but not in the IM_OC scheme. A large portion of the SOA that was condensed on soot in IM is mixed with sulfate in IM_OC, and the SOA associated with both fSoot and bSoot decreases, especially in strong source areas such as China and the middle of Africa (*SI Appendix*, Fig. S1). As a result, the percentage of SOA mixed with soot decreases from 34 to 5.5%. In IM_OC, more SOA is internally mixed with sulfate which accounts for more than 90% of the total SOA. Thus, the amount of SOA associated with sulfate aerosols is larger in IM_OC than in IM.

Table 1. Summary of the average burden, composition percentage, and radiative effect of SOA in each scheme

Parameter	EM	IM	IM_OC
SOA burden, mg m^{-2}	2.13 (0.40~18.1)	2.13 (0.41~17.6)	2.03 (0.41~17.2)
$SOASO_4^{2-}$ (nucleation)	/	2.08% (0.29~6.13%)	2.90% (0.47~7.77%)
$SOASO_4^{2-}$ (Aitken)	/	14.0% (3.30~25.9%)	20.7% (5.81~40.5%)
$SOASO_4^{2-}$ (accumulation)	/	50.1% (29.5~78.6%)	70.6% (49.6~83.7%)
$SOASO_4^{2-}$ (fossil fuel)	/	18.1% (3.58~39.0%)	2.99% (0.61~6.58%)
SOAsoot (biomass burning)	/	15.6% (3.13~41.9%)	2.55% (0.34~8.07%)
SOAother (sea salt + dust)	/	0.19% (0.02~1.26%)	0.27% (0.05~1.63%)
DRE, W m^{-2}	−0.688 (−2.54~−0.114)	−0.280 (−1.80~−0.012)	−0.249 (−1.69~−0.022)
AIE, W m^{-2}	−0.723 (−2.830~0)	−0.032 (−0.112~0)	−0.036 (−0.130~0)

Maximum and minimum values are given in parentheses. /, not available.

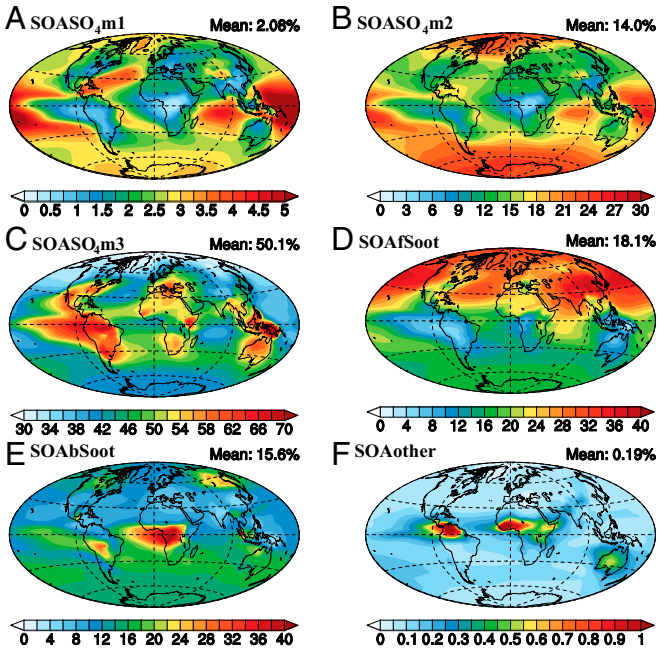

Fig. 1. Percentage of SOA internally mixed with sulfate in the nucleation (*A*), Aitken (*B*), and accumulation (*C*) modes, fSoot (*D*), bSoot (*E*), and other aerosols (dust and sea salt) (*F*) in the IM scheme.

Because of the different mixing states and distribution schemes for SOA, the model calculates different burdens and surface concentrations for each scheme (*SI Appendix*, Fig. S2). This difference in SOA burden is caused by differences in deposition and transport due to changes in hygroscopicity and particle size. For example, the hygroscopicity of the SOA mixture is larger when SOA is internally mixed with soluble hygroscopic sulfate in the accumulation mode compared with that for externally mixed SOA. Therefore, IM of SOA causes a larger scavenging efficiency than that from EM, which leads to a higher wet deposition. This also causes much more SOA to be scavenged near the precursor source areas in the IM scheme as seen mainly in the tropical continental areas (*SI Appendix*, Fig. S3). As a result, much less SOA is transported to remote areas in the IM scheme than the EM scheme, which leads to smaller wet deposition in remote areas. In addition, when SOA is internally mixed with fSoot and dust, the hygroscopicity of the mixture is less than that of SOA in the EM scheme. This causes a decrease in wet deposition and an increase in SOA burden in the regions where there is a relatively high percentage of SOA mixed with fSoot. While dry deposition removes much less SOA in the source areas than does wet deposition, the dry deposition rate of SOA also increases due to the increased particle size when SOA is internally mixed with sulfate in the accumulation mode as well as with some dust and sea salt particles in larger sizes. Mixing changes between the IM and IM_OC scheme cause the burden of SOA in the IM_OC scheme to be less than that in the IM scheme in all areas (see discussion in *SI Appendix*, section S2).

Influence of Mixing on the Radiative Effects of SOA. The radiative effect of SOA was calculated from the difference in the net incoming radiation with and without SOA at the top of atmosphere for all-sky conditions. The DRE due to SOA is always a net cooling, especially in regions with high emissions of SOA precursors like South America and central Africa and their downwind regions (Fig. 2). However, the magnitude of the DRE due to SOA is influenced by the mechanism of formation. When SOA is changed from EM with other aerosols to IM, the global average DRE is reduced from −0.69 to −0.28 W m^{-2} for several reasons (*SI Appendix*, Fig. S4). First, the change of SOA from EM to IM reduces the total particle number, resulting in a smaller total aerosol surface area in the atmosphere. Second, the IM of SOA with soot increases its absorption coefficient (8, 29), causing a total increase in absorption of 0.12 W m^{-2} (*SI Appendix*, Fig. S5). In addition, as noted above, the burden of SOA decreases in most tropical areas of the world, which directly decreases the DRE. Finally, the IM of SOA can reduce the hygroscopicity of a more hygroscopic particle like sulfate, which in turn results in less absorption of water and less-efficient scattering (10). Changes in the mass fraction of absorbing material within different aerosols also explain why the DRE for IM_OC is larger than that for IM by 0.031 W m^{-2} on average (see discussion in *SI Appendix*, section S3 and Fig. S4).

The AIE due to SOA is much more sensitive to the formation mechanism of SOA than is the DRE. The global average AIE of SOA is negative (i.e., a cooling effect) for all three schemes in this study. The largest areas of cooling include the continental regions with high SOA burdens and off the west coasts of those areas where stratiform clouds occur. The inclusion of SOA in the EM scheme results in a global annual mean AIE of −0.723 W m^{-2} with a peak cooling of −2.8 W m^{-2} off the coasts in the tropics, while the average AIE is only −0.036 W m^{-2} for the IM scheme (Fig. 2). When SOA forms as EM, the aerosol number concentration evidently increases. Some of these independent particles are able to act as cloud condensation nuclei (CCN), which increases the global average cloud droplet number concentration (CDNC) by 7.80 cm^{-3}. In the IM scheme all SOA is internally mixed with other aerosols, which results in a strongly decreased aerosol number concentration compared with the EM scheme, although the aerosol burden for the two schemes is similar. For the IM scheme, the condensation of SOA allows preexisting particles to grow to larger sizes, increasing the potential to form CCN. SOA associates preferentially with aerosols with a larger mass (thermodynamic effect) or surface area (kinetic effect), resulting in a large amount of SOA internally mixed with sulfate in the accumulation mode. However, most of the sulfate particles

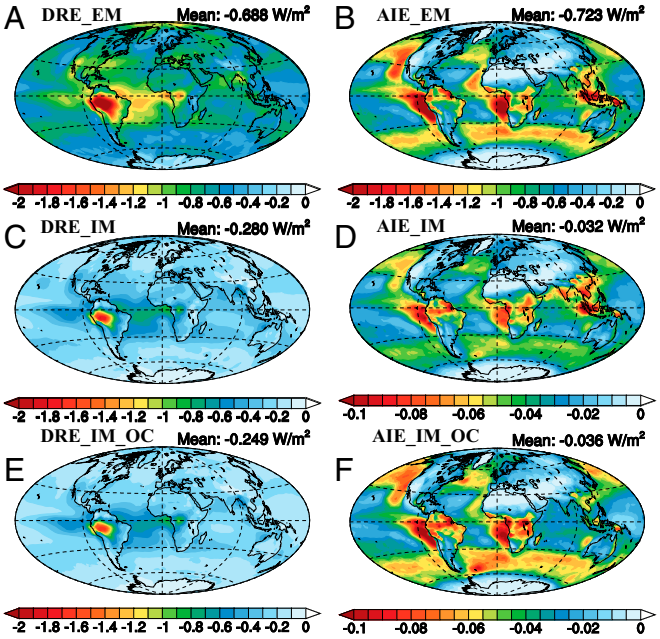

Fig. 2. Present-day DRE and AIE due to SOA in EM (*A* and *B*), IM (*C* and *D*), and IM_OC (*E* and *F*) (W m^{-2}). The global average radiative effect of SOA is given in each figure label.

Table 2. Direct and first IRF and the difference in the composition burden in FUCLI and FUALL scheme

Parameter	Scenario or SOA type	FUCLI*	FUALL†
DRF, W m^{-2}	21M20C (2100 Met + 2000 Conc)	−0.0028	−0.0028
	20M21C (2000 Met + 2100 Conc)	−0.0434	−0.0226
	21M21C (2100 Met + 2100 Conc)	−0.0470	−0.0251
First IRF, W m^{-2}	21M20C (2100 Met + 2000 Conc)	−0.0006	−0.0006
	20M21C (2000 Met + 2100 Conc)	−0.0028	−0.0414
	21M21C (2100 Met + 2100 Conc)	−0.0035	−0.0426
Difference of composition burden (future-present day), mg m^{-2}	$SOASO_4^{2-}$ (nucleation)	−0.011	−0.013
	$SOASO_4^{2-}$ (Aitken)	−0.001	0.094
	$SOASO_4^{2-}$ (accumulation)	0.295	−0.043
	SOASoot (fossil fuel)	0.074	0.053
	SOASoot (biomass burning)	0.151	0.049
	SOAother (sea salt + dust)	0.002	0.005
	Total SOA	0.510	0.145

*FUCLI is the scheme with only climate and CO_2 change in the future.
†FUALL is the scheme with the combined effects of changes in climate, anthropogenic emissions, and land use in the future.

in the accumulation mode are already CCN, so the IM of SOA with these particles only leads to an increase in the radius of CCN-sized particles without increasing the droplet numbers substantially. Only the small amount of SOA condensed onto smaller particles like sulfate in the nucleation and Aitken modes makes a substantial contribution toward increasing the CDNC. On the other hand, the IM with SOA alters the hygroscopicity of preexisting particles (34). SOA can make hydrophobic particles such as dust more hydrophilic, providing an additional source of new CCN, but they can also reduce the hygroscopicity of more hydrophilic particles like sulfate and sea salt. The net change to the CCN concentration therefore reflects the integrated competition between the growth in particle size and the change in hygroscopicity. As a result, in the IM scheme SOA only increases the CDNC by 0.35 cm^{-3}. The small influence on CDNC from SOA in the IM scheme (*SI Appendix*, Fig. S6) leads to a smaller AIE due to SOA. The difference in the AIE between the IM_OC and IM scheme is very small but distributed unevenly (see discussion in *SI Appendix*, section S4 and Fig. S4).

The RF of SOA Due to Future Changes in Climate and CO_2. Two future cases were examined using the IM distribution scheme: one for the future SOA burden due to climate change and increases in CO_2 (FUCLI) and one that included future changes in climate, all anthropogenic emissions, and land use (FUALL). Both cases followed the Representative Concentration Pathway (RCP) 8.5, but led to very different changes in natural SOA precursor emissions (32). Our previous study (32) showed that the FUCLI scenario results in a large increase in SOA mass (25%) due to the increased surface temperatures and CO_2, which cause an increase in SOA precursor emissions (primarily isoprene). However, if we also account for changes in land use and anthropogenic emissions (FUALL), the SOA mass increase is only 2% (32). In the current model, in the FUCLI scenario the burden of SOA increases by 23.9%, while the increase is 6.8% for FUALL. For FUCLI, the SOA burden increases in most tropical and subtropical regions but decreases in some places like Australia, where increased precipitation removes more SOA in the future (*SI Appendix*, Fig. S7). Since most anthropogenic emissions do not change in this simulation, sulfate in the accumulation mode is still the dominant aerosol type with which most SOA is associated. The burden of SOA condensed on bSoot increases by 0.151 mg m^{-2}, which is smaller than the SOA associated with sulfate in accumulation mode (which increases by 0.295 mg m^{-2}), while the SOA associated with fSoot increases by 0.074 mg m^{-2} (Table 2). This is due to the fact that the natural SOA precursors increase much more in tropical regions and there is far more bSoot than fSoot in the tropics, although SOA associated with fSoot increases more than that on bSoot in Europe, east China, and India which are important emission source areas for fSoot (*SI Appendix*, Fig. S7).

Three RF cases were examined for each future scheme to identify the relative role of changes in meteorology versus changes in SOA. 21M20C considered only the change in meteorology in 2100 when calculating the radiative effect, while 20M21C considered only the change in SOA. The 21M21C case included both the change in meteorology and SOA. The 2100 meteorological conditions increase the direct radiative forcing (DRF) by −0.0028 W m^{-2} and the first indirect forcing (IRF) by −0.0006 W m^{-2} (Table 2). These changes are mainly caused by the difference in clouds between the future and present day. For liquid water clouds, cloud optical depth, and liquid water path decrease in most continental regions, especially in Europe, east- and south Asia and the eastern North and South America, while they increase over much of ocean and in coastal regions (*SI Appendix*, Fig. S8). The decrease of cloud properties strengthens the DRE of SOA but weakens the AIE, which leads to regional changes in the DRF and IRF with opposite signs (*SI Appendix*, Fig. S9). The RF caused by the change in SOA concentration is larger than the RF caused by the change in meteorology. The SOA burden change caused by climate change results in a DRF of −0.043 W m^{-2} and an IRF of −0.0028 W m^{-2} in the simulation 20M21C case (*SI Appendix*, Fig. S9). The increase of the particle size due to increased SOA leads to an 11% increase in the SOA aerosol optical depth (AOD). The DRF is negative and correlates with the increase of SOA and AOD in most regions where the SOA burden increases. However, DRF is positive in east China as the result of increased radiation absorption due to the mixing of SOA with fSoot. Increased SOA due to climate change also increases the global average CDNC due to SOA by 14% since more aerosols are able to grow to a size able to act as CCN. However, much of the increased SOA is mixed with sulfate in the accumulation mode. Since these aerosols are already CCN, the increase in the SOA only leads to an 8.8% increase in the AIE, despite the 24% increase in total SOA. The 21M21C result is close to the sum of the changes due to meteorology (21M20C) and SOA concentrations (20M21C). In total, climate and CO_2 changes cause a direct forcing of −0.047 W m^{-2} and a first indirect forcing of −0.0035 W m^{-2}, which increases the radiative effect of SOA by 16% (Fig. 3).

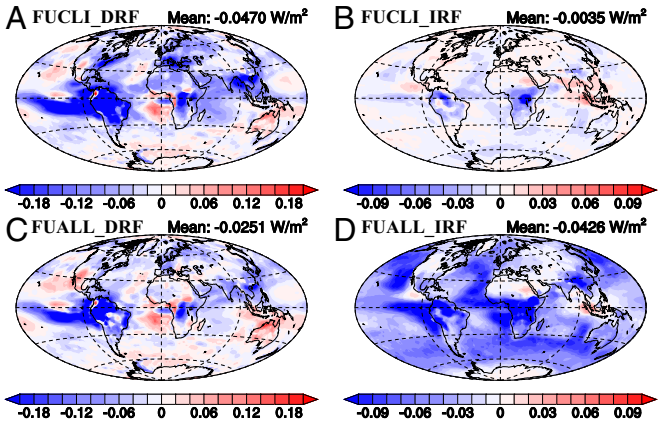

Fig. 3. Spatial distribution of DRF and first IRF in the FUCLI scheme due to changes in climate and CO_2 (*A* and *B*) and in the FUALL scheme due to changes in climate, all anthropogenic emissions, and land use (*C* and *D*). The global average RF of SOA is given in each figure label.

The RF of SOA Due to All Future Changes. When climate change, anthropogenic emissions, and land use all change as a result of the RCP8.5 scenario, SOA only increases by 6.8%. This smaller increase is associated with a net decrease in SOA burden due to land-use change and anthropogenic emissions (32). The largest increase in burden occurs in the northwest of South America and its outflow over the Pacific Ocean while a decrease in the burden occurs in the eastern Amazon rainforest, United States, and east China (*SI Appendix*, Fig. S10). Although the change in the global burden of SOA in the future is not as significant as that due to only CO_2 and climate change, the change in the mixing state of SOA is noticeable. As shown in Table 2, compared with the present day there is 32% more SOA mixed with sulfate in the Aitken mode while SOA mixed with sulfate in accumulation mode decreases. The anthropogenic emissions of sulfur dioxide (a precursor to sulfate) and particles are projected to decline in the future, leading to a smaller percentage of sulfate in large sizes due to reduced condensation and coagulation. Moreover, the cleaner environment of the future with its reduced condensation sink promotes nucleation of sulfate particles, which grow to the Aitken mode. As a result, the mass and surface-area percentages of sulfate in the Aitken mode increase by 2.6 and 4.8%, respectively, while the percentage of sulfate in the accumulation mode decreases. Thus, the percentage of SOA mixed with sulfate in the Aitken mode increases to 17% (from 14% in present day) and that of SOA mixed with sulfate in the accumulation mode decreases to 45% (from 50% in present day).

These changes in the distribution of SOA for the FUALL case lead to substantial changes in the future forcing compared with the FUCLI case. The difference in the SOA concentration between the future and present day causes only –0.023 W m^{-2} DRF in the 20M21C case, which is only 52% of that caused by climate and CO_2 change in the FUCLI scheme. The spatial distribution of the DRF follows that of the change of SOA burden (compare *SI Appendix*, Figs. S10*A* and S11*A*). In contrast, the IRF is substantially larger (more negative) in the FUALL case (–0.04 W m^{-2}) than in the FUCLI case (–0.003 W m^{-2}).This difference is caused by the addition of SOA to sulfate in the Aitken mode which causes a substantial increase in CCN even though the increase in SOA burden is significantly smaller than that in the FUCLI case. As a result, the CDNC due to SOA increases by 59%. For the combined effect of changes in meteorology and SOA in the future, the DRF and IRF of SOA are –0.025 and –0.043 W m^{-2}, respectively (Fig. 3). Even though the increase in the burden of SOA is much larger in the FUCLI scheme, the total RF of SOA is much larger in the FUALL scheme due to the notable change of mixing distribution for SOA.

Implications and Discussion

This study demonstrates the importance of the distribution of SOA and its association with other aerosol types for the correct calculation of its radiative effects. The size distribution of SOA is an important factor which determines the activation of aerosol particles to form cloud droplets and therefore indirect climate effects. The mixing state and distribution of SOA in aerosols determines the importance of SOA in future climate change. Due to emissions reductions, the RF of anthropogenic aerosols is expected to be positive and on the order of 0.1~0.2 W m^{-2} in the future (35, 36). Here we show that changes in SOA may act to offset some of this positive forcing. However, while SOA increases in the future primarily as a result of climate change, its RF is only able to mask a small percentage of the RF associated with greenhouse gases in the RCP 8.5 scenario, which is ~8.5 W m^{-2}. Thus, we cannot rely on increases in natural SOA emissions to mask much of the future warming caused by greenhouse gas increases.

The calculations presented here are limited by the mechanisms for SOA formation represented in the underlying model. The nucleation of SOA from the products of α-pinene oxidation (37, 38) is excluded, which possibly leads to an underestimation of the AIE. A recent paper also indicates that particles with a mass ratio of nonblack carbon to black carbon less than 1.5 have no absorption enhancement while significant absorption enhancement occurs when the ratio is greater than 3 (29). Adding such an effect to our model would influence our estimate of the DRE for particles with IM. In addition, the sensitivity study for the distribution of SOA associated with OC (based on the finding from ref. 33) is simplified. As new knowledge is developed, our simplified treatment will need to be expanded, based on knowledge of the physical and chemical characteristics of aerosols and their mixing with SOA.

Methods

This study employed Community Earth System Model Version 1.2.2 coupled with the University of Michigan IMPACT aerosol model to simulate SOA concentrations. Besides SOA, five EM aerosol types (i.e., pure-sulfate aerosol, soot from fossil fuel, soot from biomass burning, dust, and sea salt) are treated. Fifteen separate aerosol species were simulated in the model, including pure sulfate in three modes (i.e., nucleation, Aitken and accumulation), soot from biomass burning [i.e., primary organic aerosol and black carbon (BC) from biomass burning (bOC and bBC)], soot from fossil-fuel burning (i.e., primary organic carbon and black carbon), and dust and sea salt, which were each carried in four separate bins with varying radii. The detailed model description and setup can be found in ref. 39. The explicit gaseous-phase chemical mechanism for the formation of semivolatile organic products, including the oxidation of isoprene, α-pinene and aromatics, is described in refs. 15 and 40. Lower-volatility compounds like oligomers form when semivolatile organics are incorporated into the aerosol phase. SOA formation from aqueous-phase reactions of glyoxal and methyglyoxal and the kinetic uptake of IEPOX, glyoxal, and methylgloxal were included as described for case 1 in ref. 16. Each model simulation was performed for 5 y with a 0.5 y spin-up. The model ability to simulate the formation of SOA has previously been evaluated by comparison with measurements (15, 16, 32).

An off-line radiative transfer model was used to calculate aerosol optical properties and cloud droplet activation, and thus to estimate the DRE and AIE. We used 5 y of monthly average aerosol concentrations together with the first year of four hourly meteorological conditions to calculate the radiative effects (41, 42). The mixing state of aerosol was taken from that calculated in the IMPACT model. The refractive indices and hygroscopicity of particles with IM within each aerosol type were calculated by volume weighting of each of the individual aerosol species. Köhler theory together with the soluble fraction on each aerosol type was used to predict the amount of water, which was also considered to affect the particle size and refractive indices. The model was introduced in detail by refs. 12 and 43.

Three simulation schemes for present day were designed to quantify the radiative effect of SOA using different formation mechanisms. The EM scheme assumed that all SOA is formed as an external mixture, except that gaseous sulfate is allowed to condense on SOA aerosol and pure-sulfate aerosol may coagulate with SOA. This is the simplest and most common way to calculate the radiative effects of SOA in previous studies (12–14). The IM scheme was based on the mechanism used in the IMPACT model for SOA

formation. As described in refs. 15 and 16, SOA is formed from the thermodynamic process of gas-phase partitioning of semivolatile species followed by oligomer formation within aerosols, from the kinetic formation of SOA on the surface of acidic aerosol particles, and from the formation of SOA via aqueous formation within cloud drops. Thermodynamic formation contributes SOA to preexisting aerosols based on the amount of organics present in the preexisting aerosols (44). The formation of SOA on the surface of acidic aerosol particles is distributed according to the available surface area of these aerosols (45–47). The formation of SOA via aqueous-phase formation within drops is distributed to the particles that act as CCN within drops (similar to the distribution of sulfate formed within drops). While our original publications (15, 16) described several different versions of these chemical mechanisms, here we only treat case 1 in ref. 16. We refer the reader to refs. 15 and 16 for a description of the range of concentrations that result from different treatments for the formation mechanism of SOA as well as for an evaluation of the predicted concentrations. The characteristics of preexisting aerosols that are mixed with SOA, including size distribution, density, and refractive indices, can be found in ref. 12. The detailed method used to distribute SOA formed from thermodynamic, kinetic, and aqueous-phase production, respectively, is described in *SI Appendix*, section S1.

A recent measurement has indicated that primary OC from anthropogenic sources are nonliquid even at high RH and exist in an EM state in the Amazon (33). We tested the effect of this assumption in the IM_OC scheme which was developed by modifying the IM scheme to include the assumption of no SOA partitioning to primary OC via the thermodynamic process. The setup for simulation in IM_OC was similar to that in IM except that the mass concentration of SOA condensed on OC was calculated using *SI Appendix*, Eq. **S2** instead of *SI Appendix*, Eq. **S1**.

The concentration of SOA and its DRE and AIE in the future was modeled using the SOA formation mechanism from the IM scheme together with the RCP8.5 scenario for year 2100 (48). The RF of SOA in the future was defined as the difference between the radiative effect of SOA in the future and present day.

ACKNOWLEDGMENTS. Computer time was provided by the National Center for Atmospheric Research Computational Information Systems Laboratory. We are grateful for funding from the NASA Atmospheric Composition Modeling and Analysis Program under Grant NNX15AE34G as well as NSF 1540954. G.L. was supported by the Climate Model Development and Validation activity funded by the Office of Biological and Environmental Research in the US Department of Energy Office of Science.

1. Hallquist M, et al. (2009) The formation, properties and impact of secondary organic aerosol: Current and emerging issues. *Atmos Chem Phys* 9:5155–5236.
2. Jimenez JL, et al. (2009) Evolution of organic aerosols in the atmosphere. *Science* 326: 1525–1529.
3. Scott CE, et al. (2014) The direct and indirect radiative effects of biogenic secondary organic aerosol. *Atmos Chem Phys* 14:447–470.
4. Tsigaridis K, et al. (2014) The AeroCom evaluation and intercomparison of organic aerosol in global models. *Atmos Chem Phys* 14:10845–10895.
5. Jacobson MZ (2001) Strong radiative heating due to the mixing state of black carbon in atmospheric aerosols. *Nature* 409:695–697.
6. Zaveri RA, Barnard JC, Easter RC, Riemer N, West M (2010) Particle-resolved simulation of aerosol size, composition, mixing state, and the associated optical and cloud condensation nuclei activation properties in an evolving urban plume. *J Geophys Res* 115:D17210.
7. Koch D, et al. (2009) Evaluation of black carbon estimations in global aerosol models. *Atmos Chem Phys* 9:9001–9026.
8. Moffet RC, Prather KA (2009) In-situ measurements of the mixing state and optical properties of soot with implications for radiative forcing estimates. *Proc Natl Acad Sci USA* 106:11872–11877.
9. Pratt KA, Prather KA (2010) Aircraft measurements of vertical profiles of aerosol mixing states. *J Geophys Res* 115:D11305.
10. Cahill JF, Suski K, Seinfeld JH, Zaveri RA, Prather KA (2012) The mixing state of carbonaceous aerosol particles in northern and southern California measured during CARES and CalNex 2010. *Atmos Chem Phys* 12:10989–11002.
11. Yang F, et al. (2009) Single particle mass spectrometry of oxalic acid in ambient aerosols in Shanghai: Mixing state and formation mechanism. *Atmos Environ* 43: 3876–3882.
12. Lin G, et al. (2014) Radiative forcing of organic aerosol in the atmosphere and on snow: Effects of SOA and brown carbon. *J Geophys Res Atmos* 119:7453–7476.
13. Yin C, et al. (2015) Assessment of direct radiative forcing due to secondary organic aerosol over China with a regional climate model. *Tellus B Chem Phys Meterol* 67: 24634.
14. Goto D, Takemura T, Nakajima T (2008) Importance of global aerosol modeling including secondary organic aerosol formed from monoterpene. *J Geophys Res* 113: D07205.
15. Lin G, Penner JE, Sillman S, Taraborrelli D, Lelieveld J (2012) Global modeling of SOA formation from dicarbonyls, epoxides, organic nitrates and peroxides. *Atmos Chem Phys* 12:4743–4774.
16. Lin G, Sillman S, Penner JE, Ito A (2014) Global modeling of SOA: The use of different mechanisms for aqueous-phase formation. *Atmos Chem Phys* 14:5451–5475.
17. Adachi K, Buseck PR (2008) Internally mixed soot, sulfates, and organic matter in aerosol particles from Mexico City. *Atmos Chem Phys* 8:6469–6481.
18. Freney EJ, Adachi K, Buseck PR (2010) Internally mixed atmospheric aerosol particles: Hygroscopic growth and light scattering. *J Geophys Res Atmos* 115:D19210.
19. Heald CL, et al. (2008) Predicted change in global secondary organic aerosol concentrations in response to future climate, emissions, and land use change. *J Geophys Res Atmos* 113:D05211.
20. Pye HOT, Seinfeld JH (2010) A global perspective on aerosol from low-volatility organic compounds. *Atmos Chem Phys* 10:4377–4401.
21. O'Donnell D, Tsigaridis K, Feichter J (2011) Estimating the direct and indirect effects of secondary organic aerosols using ECHAM5-HAM. *Atmos Chem Phys* 11:8635–8659.
22. Makkonen R, et al. (2012) BVOC-aerosol-climate interactions in the global aerosol-climate model ECHAM5.5-HAM2. *Atmos Chem Phys* 12:10077–10096.
23. D'Andrea SD, et al. (2015) Aerosol size distribution and radiative forcing response to anthropogenically driven historical changes in biogenic secondary organic aerosol formation. *Atmos Chem Phys* 15:2247–2268.
24. Yu F (2011) A secondary organic aerosol formation model considering successive oxidation aging and kinetic condensation of organic compounds: Global scale implications. *Atmos Chem Phys* 11:1083–1099.
25. Riipinen I, et al. (2011) Organic condensation: A vital link connecting aerosol formation to cloud condensation nuclei (CCN) concentrations. *Atmos Chem Phys* 11: 3865–3878.
26. Pierce JR, et al. (2011) Quantification of the volatility of secondary organic compounds in ultrafine particles during nucleation events. *Atmos Chem Phys* 11: 9019–9036.
27. Jokinen T, et al. (2015) Production of extremely low volatile organic compounds from biogenic emissions: Measured yields and atmospheric implications. *Proc Natl Acad Sci USA* 112:7123–7128.
28. Rap A, et al. (2013) Natural aerosol direct and indirect radiative effects. *Geophys Res Lett* 40:3297–3301.
29. Liu DT, et al. (2017) Black-carbon absorption enhancement in the atmosphere determined by particle mixing state. *Nat Geosci* 10:184–188.
30. Bond TC, Habib G, Bergstrom RW (2006) Limitations in the enhancement of visible light absorption due to mixing state. *J Geophys Res Atmos* 111:D20211.
31. Westervelt DM, Horowitz LW, Naik V, Golaz JC, Mauzerall DL (2015) Radiative forcing and climate response to projected 21st century aerosol decreases. *Atmos Chem Phys* 15:12681–12703.
32. Lin G, Penner JE, Zhou C (2016) How will SOA change in the future? *Geophys Res Lett* 43:1718–1726.
33. Bateman AP, et al. (2017) Anthropogenic influences on the physical state of submicron particulate matter over a tropical forest. *Atmos Chem Phys* 17:1759–1773.
34. Mochida M, et al. (2006) Relationship between hygroscopicity and cloud condensation nuclei activity for urban aerosols in Tokyo. *J Geophys Res Atmos* 111:D23204.
35. Chen W-T, Liao H, Seinfeld JH (2007) Future climate impacts of direct radiative forcing of anthropogenic aerosols, tropospheric ozone, and long-lived greenhouse gases. *J Geophys Res* 112:D14209.
36. Shindell DT, et al. (2013) Radiative forcing in the ACCMIP historical and future climate simulations. *Atmos Chem Phys* 13:2939–2974.
37. Zhang X, et al. (2015) Formation and evolution of molecular products in α-pinene secondary organic aerosol. *Proc Natl Acad Sci USA* 112:14168–14173.
38. Kirkby J, et al. (2016) Ion-induced nucleation of pure biogenic particles. *Nature* 533: 521–526.
39. Zhou C, Penner JE (2014) Aircraft soot indirect effect on large-scale cirrus clouds: Is the indirect forcing by aircraft soot positive or negative? *J Geophys Res Atmos* 119: 11303–11320.
40. Ito A, Sillman S, Penner JE (2007) Effects of additional nonmethane volatile organic compounds, organic nitrates, and direct emissions of oxygenated organic species on global tropospheric chemistry. *J Geophys Res Atmos* 112:D06309.
41. Penner JE, Xu L, Wang M (2011) Satellite methods underestimate indirect climate forcing by aerosols. *Proc Natl Acad Sci USA* 108:13404–13408.
42. Penner JE, Zhou C, Xu L, Wang MH (2011) Reply to Quaas et al.: Can satellites be used to estimate indirect climate forcing by aerosols? *Proc Natl Acad Sci USA* 108: E1100–E1101.
43. Xu L, Penner JE (2012) Global simulations of nitrate and ammonium aerosols and their radiative effects. *Atmos Chem Phys* 12:9479–9504.
44. Pankow JF (2003) Gas/particle partitioning of neutral and ionizing compounds to single and multi-phase aerosol particles. 1. Unified modeling framework. *Atmos Environ* 37:3323–3333.
45. Liggio J, Li SM, McLaren R (2005) Reactive uptake of glyoxal by particulate matter. *J Geophys Res Atmos* 110:D10304.
46. Fu TM, Jacob DJ, Heald CL (2009) Aqueous-phase reactive uptake of dicarbonyls as a source of organic aerosol over eastern North America. *Atmos Environ* 43:1814–1822.
47. Fu TM, et al. (2008) Global budgets of atmospheric glyoxal and methylglyoxal, and implications for formation of secondary organic aerosols. *J Geophys Res Atmos* 113: D15303.
48. van Vuuren DP, et al. (2011) The representative concentration pathways: An overview. *Clim Change* 109:5–31.